Effect of fabric architecture, compaction and permeability on through thickness thermoplastic melt impregnation

Studer, Julia; Dransfeld, Clemens; Jauregui Cano, Jon; Keller, Andre; Wink, Marianne; Masania, Kunal; Fiedler, Bodo

DOI
10.1016/j.compositesa.2019.04.008

Publication date
2019

Document Version
Accepted author manuscript

Published in
Composites Part A: Applied Science and Manufacturing

EFFECT OF FABRIC ARCHITECTURE, COMPACTION AND PERMEABILITY ON THROUGH THICKNESS THERMOPLASTIC MELT IMPREGNATION

Julia Studer[1,4*], Clemens Dransfeld[1,5*], Jon Jauregui Cano[1], Andre Keller[1], Marianne Wink[2], Kunal Masania[3], Bodo Fiedler[4]

[1]Institute of Polymer Engineering, FHNW University of Applied Sciences and Arts Northwestern Switzerland, Klosterzelgstrasse. 2, 5210 Windisch, Switzerland;

[2]Institute of Polymer Nanotechnology, FHNW University of Applied Sciences and Arts Northwestern Switzerland, Klosterzelgstrasse. 2, 5210 Windisch, Switzerland;

[3]Complex Materials Group, Department of Materials, ETH Zürich, 8093 Zurich, Switzerland

[4]Institute of Polymer Composites, Hamburg University of Technology, Denickestrasse 15, 21073 Hamburg, Germany

[5]present address: Faculty of Aerospace Engineering, TU Delft, Kluyverweg 1, 2629 HS Delft, the Netherlands

Corresponding authors: julia.studer@fhnw.ch, c.a.dransfeld@tudelft.nl

Abstract

To reduce the cycle time of structural, automotive thermoplastic composites, we investigated the potential of direct thermoplastic melt impregnation of glass fabrics using an injection moulding process. At the high pressures that occur during the process, the effect of the fabric architecture on the impregnation, compaction, volume fraction and permeability of two unidirectional fabrics was studied. Using impregnation experiments with a low viscosity PA6 melt, we identified a favourable processing window resulting at an impregnation time of 5 min. The impregnation experiments with thermoplastic melts demonstrate that textile architectures promoting dual scale flow during impregnation are favourable for complete filling. Based on our findings, thermoplastic compression resin transfer moulding is an efficient processing route for automated production of composite parts with a high fibre volume fraction, if the fabric architecture is adapted for higher processing pressures and by fully utilising dual scale flow.

Keywords E. Manufacturing / Processing: Injection moulding, Compression resin transfer moulding, Fibre tow infiltration, Liquid composite moulding

1 Introduction

Liquid composite moulding processes, such as resin transfer moulding (RTM) [1-4] and compression resin transfer moulding (CRTM) [5-8] are widely established in industry to fabricate composite materials [9]. These processes typically utilise very short impregnation distances and/or require low viscosity resins, to achieve reasonable processing times, e.g., thermoset resins or reactive thermoplastic resins with a viscosity below 1 Pas are usually used to produce composite structures today [10, 11].

Compared to thermosets, thermoplastic matrix materials have significant advantages such as recyclability [12], shorter cycle times and high fracture toughness. They also offer alternative joining processes such as welding [13], making them a highly attractive option for automated large volume production. Thermoplastic melts, however, usually have a viscosity above 200 Pas, being 100-1000 times higher than thermoset resins. This significantly increases impregnation time of fabrics, especially if high a fibre volume fraction, Vf, is desired in the final part. For industries such as the automotive, to remain cost-effective, fast and reliable, new processes are highly sought after.

State of the art manufacturing processes of continuous fibre thermoplastic composites in structural applications are primarily based on the tape laying of pre-impregnated tapes [14, 15], and over-injection of pre-impregnated organic sheets [16-18]. Both processes involve semi-finished products where the textile is pre-impregnated with a thermoplastic resin. For example, with the tape laying process, a fully impregnated and pre-consolidated tape is heated locally and placed in defined path by a robot head, which also applies the consolidation pressure. In the over-injection process, a pre-impregnated organic sheet is preheated and placed in the mould for injection moulding where it is simultaneously formed and often over-moulded to add functionality. This process results in functional net-shaped parts, which can include details such as clamps, holes or stiffeners. Both of these approaches use semi-finished products to overcome the high viscosity of the thermoplastic melt by melding adjacent layers rather than relying on flow to impregnate the composite material.

An alternative approach to overcome these typical challenges is the use of very low viscosity monomers and in situ anionic ring opening polymerisation process of materials such as caprolactam [19]. This polymerisation method is, however, highly sensitive to residual moisture content and contaminations and hence difficult to control in an industrial liquid composite moulding scenario [20].

With novel engineering thermoplastic materials of low melt viscosities becoming commercially available [21], direct impregnation processes of composites are gaining attention. Such polymers have been previously used for pultrusion [22] and for RTM [23-25] processes. Despite their lower viscosity, it was shown that considering the typical flow length of structural components, the one to two magnitudes higher viscosity compared to typical thermoset resins means that in-plane impregnation of large structures remains a challenge. A reduction of flow length by means of through the thickness impregnation using, for example, CRTM is therefore attractive to produce large structures in an efficient manner. By implementing the process on injection moulding machines that are widely used in industry, impregnation and net shaping with functionalities could be realised in one production step. In the proposed thermoplastic polymer gap injection CRTM process (TP CRTM), shown schematically in Fig. 1a, the molten polymer is injected from the top into a gap above the dry fabric in a hot mould. Through a compression stroke of the machine, the fabric is impregnated with polymer with a near uniform pressure acting on the surface of the fabric. After the impregnation is complete, the mould may be cooled, the part ejected and the cycle may be repeated. Vario-thermal injection moulding processes, although with smaller ΔT, are already widely used in industry for e.g. optical parts in automotive or the replication of microstructures. Possible heating concepts include external radiation or induction heating of the mould, and a proper thermal heat flow design to minimise the portions of the tool that will experience the vario-thermal cycle.

The impregnation time of a liquid resin or polymer melt flowing through a fibre bed can be estimated using Darcy's Law [26]. It describes the flow of a Newtonian fluid in a rigid porous medium, Eq. (1):

$$u = -\frac{K}{\eta}\nabla P \qquad (1)$$

where u is the volume averaged velocity of the fluid, K the fabric permeability, η the fluid viscosity and ∇P the pressure gradient. For a one-dimensional saturated flow, Eq. (1) can be expressed as Eq. (2):

$$\frac{q}{A} = \frac{K\Delta p}{L\eta} \tag{2}$$

Where q is the volume flow, η is the fluid viscosity, L is the impregnation length, Δp is the pressure difference and A is the impregnation area.

For the estimation of the flow front position at time t L(t) under the assumption of slug flow and neglecting the capillary pressure, ∇p can be expressed as Eq. (3):

$$\nabla p = \frac{p_f - p_{ap}}{L(t)} = \frac{\Delta p}{L(t)} \tag{3}$$

Where p_f is the pressure at the flow front and p_{ap} the applied pressure.

The flow front velocity, u_f, is related to u as follows Eq. (4):

$$u_f = \frac{u}{(1 - Vf)} \tag{4}$$

Where Vf is the fibre volume fraction. Combining Eq. (1), (3) and (4) leads to Eq. (5):

$$\frac{dL}{dt} = \frac{K\Delta p}{(1 - Vf)\eta L(t)} \tag{5}$$

When integrating Eq. (5), an expression to estimate the impregnation time for a one-dimensional flow can be derived Eq. (6):

$$t_{imp} = \frac{(1 - Vf)\eta\, L^2}{2K\Delta p} \tag{6}$$

where L is the impregnation length.

The permeability is determined by Vf and in our case, the impregnation length corresponds to the thickness of the part. There is a gradient in Vf, emerging from the balance of the applied pressure and the pressure distribution between the fabric and the matrix, which can be described by Terzaghi's law [27], Eq. (7):

$$p_{ap} = \sigma_{pref} + p \quad (7)$$

where p_{ap} is the applied pressure from the mould, σ_{pref} is the preform stress and p, the fluid pressure. σ_{pref} changes during the process and spatially through the thickness, as illustrated in Fig. 1c. This results in variable Vf (Fig. 1b) and thus K depending on σ_{pref}, [5, 28] as was previously investigated for thermoset resins [5-7, 29, 30] using CRTM. This process is especially interesting for fast curing thermosets [31], offering a further reduction of cycle time to a matter of seconds. The textile architectures that are typically used for these very fast processes have a dual scale porosity through their continuous fibre tow architecture arranged into layers. These pores exist on the microscopic length scale between single fibres inside a tow and between tows on the tenths of a millimetre [10] mesoscopic scale. Due to the microscopic size of continuous pores, capillary forces can dominate the flow within the tow [32], next to the difference in permeability, which results in heterogeneous dual scale flow. Whether inter- or intra-tow flow dominates the impregnation is determined by a balance of capillary forces, local porosity, viscosity, and flow rate [33, 34].

The use of the low viscosity thermoplastic melts that are 10-100 times higher in viscosity than typical thermoset resins suggests the need for higher pressures than in thermoset CRTM. This leads to the following questions: first, is the impregnation mechanism single or dual scale, second, what is the effect of textile architecture on fabric compaction and permeability, and finally is there an attractive processing window for a cost-effective manufacturing process?

The compaction behaviour and through thickness permeability, measured with a low viscosity fluid, of two unidirectional (UD) glass fabrics were investigated at the typical fibre volume fractions resulting from the processing pressures (estimated 10 to 50 bar) that occur during the TP CRTM process. Then, we conducted impregnation experiments of these fabrics with a low viscosity polyamide to determine the impregnation mechanisms and find suitable processing parameters for low porosity. With all this information, we identify a favourable processing window for the investigated materials, and find implications for new fabric architectures that would be ideally suited for the TP CRTM process.

2 Methods

2.1 Materials

Low viscosity polyamide 6 (PA6), “Evolite® HF XS1480”, Solvay was used for the impregnation experiments. It has a melt viscosity of 40 Pas at 280 °C which decreases to 15 Pas at 300 °C (Fig. 2a) [35], and is thermally stabilised to avoid degradation during processing. Before use, the polyamide was dried in an vacuum oven at 110 °C for 12 h, then let to cool down under vacuum, and then the PA6 was immediately sealed in laminated bags to avoid humidity and changing viscosities due to degradation [36]. This procedure was suggested by the manufacturer and the humidity content was verified with an Aquatrac® 3E, Brabender Messtechnik GmbH, Germany, to be under 0.1%.

Because of the high processing temperatures, we chose UD fabrics made only from glass to avoid melting of secondary thermoplastic yarns. Two UD glass fabrics were studied and compared: A Leno weave UD fabric (1280 g/m^2, 4800 tex), FTA Albstadt GmbH, Germany, shown in Fig. 2b i) and a Two warp system UD fabric (600 g/m^2, 1200 tex), Tissa Glasweberei AG, Switzerland, shown in Fig. 2b ii).

For the permeability measurements, a silicone oil with a viscosity of 0.1 Pas was used: “Bluesil V100”, Silitech AG, Switzerland.

2.2 Dry fabric compaction

Ten layers of dry fabric were compacted between two parallel circular plates of diameter 135 mm at a constant velocity (1 mm/min) using a mechanical testing machine “Zwick Roell Z100”, Zwick GmbH & Co. KG, Germany. The machine compliance was measured and subtracted from the machine-measured displacement. Using the force and the corrected position of the machine, the pressure, P, and Vf were calculated. The compaction curves were recorded up to a pressure of 60 bar to cover the estimated process pressure.

2.3 Saturated through thickness permeability

The saturated through thickness permeability, *K*, was measured at different Vf using a custom jig, shown in Fig. 3, which is similar to those used by Michaud et al. [37] and Klunker et al. [28]. Even

though during the TP CRTM process we have unsaturated flow, due the high impregnation pressure (up to 50 bar) the effect of the capillary pressure (in the range of kPa for thermoplastic melts [38]) is minimal. The fabric stack was precompacted to a defined height of 10 mm, corresponding to the impregnation length. To obtain different values of Vf, corresponding to the processing pressures, the number of layers was varied within the same thickness. The silicone oil was injected with constant pressure from a pressure pot and enters the fabric stack from the bottom via a distribution structure and honeycomb support grid. The fabric was cut to a diameter of 79 mm on a Zünd G3 M2500, Zünd, Switzerland, but the diameter for free flow of the oil was constrained to 50 mm using thin rings from aluminium at the top and bottom of the stack to avoid race tracking. After impregnating the fabric stack, the silicone oil exited through the outlet, and was collected on a scale to calculate the volume flow, q, during the experiment. The oil pressure was measured by two sensors before and after the stack, to get the pressure difference, Δp. The pressure and mass were recorded using a LabVIEW program. With the pressure difference at inlet and outlet, the oil viscosity and the mass flow, the through thickness permeability, K can be calculated from Eq. (8) (rearranged from Darcy's law, Eq. (7)).

$$K = \frac{q\,\eta\,\Delta z}{\Delta p\,A} \tag{8}$$

where q is the volume flow, η is the viscosity, Δz is the impregnation length, Δp is the pressure gradient and A is the impregnation area.

The measurements were conducted using a silicone oil with a viscosity of 0.1 Pas. The injection pressure was set to 0.1 bar for the lowest Vf and 0.25, 0.5, and 0.8 bar for higher values of Vf.

2.4 Thermoplastic impregnation experiments

Plates with a dimension of 85 x 170 mm and of variable thickness according to target fibre volume fraction, Vf_{target}, were manufactured using a constant pressure TP CRTM process as shown in Fig. 4. Vf_{target} is the theoretical Vf assuming homogeneously distributed fibres in the matrix, and was used to calculate the amount of matrix used for a certain number of fabric layers. The mould (shown in Fig. 4a) has a vertical shut off and was sealed with high temperature tacky tape "SM5160 Tacky Tape", ITW Polymers Sealants North America, Inc. The mould was heated and cooled using a 20 ton hydraulic press "LaboPress P200T", Vogt, Germany. First, the fabric was

placed in the cold mould, and PA6 granulate was added on top of the fabric. The mould was heated without pressure until the processing temperature in the polymer was obtained, as measured by thermocouple. After pressing for a defined time and with a constant consolidation pressure (Fig. 4 b i), the mould was cooled while maintaining pressure. After demoulding, samples (15 x 30 mm) were cut from the middle of the plate (shown in Fig. 4c), to avoid occasional race tracking artefacts at the edges, then embedded and polished. To distinguish the impregnated from non-impregnated regions, the samples were consecutively embedded in a rhodamine B dyed epoxy resin according to [39]. The samples were polished with a “TegraPol21”, Struers GmbH, Switzerland, with emery paper from 240 to 2400 grit and up to 0.25 um diamond polishing solution. To analyse the samples, photographs were taken with UV and fluorescent tube light or UV light only. A UV lamp (UV hand lamp NU-6, 6 W, Herolab GmbH, Germany, 365 nm) was placed 15 cm above the sample, the camera “Nikon D810” with objective “AF-S Micro Nikkor 105 mm 1:2.8G”, Nikon Corporation, Japan, and the following camera settings were used: F10, ISO 160, and exposure time of 2.5 s for fluorescent tube and UV light, and 15 s for UV light only.

The parameters of all impregnation experiments that were investigated with the UV light optical measurements are shown summarised in Table 1.

To determine suitable processing parameters, preliminary experiments were made within a broad range of processing parameters: Temperature (260-300 °C), pressure (10-100 bar) and impregnation time (1-15 min). Together with assumptions on the industrial process and mould design, the processing window was further narrowed down based on the following assumptions: The range of Vf_{target} should be at least 0.5 for cost efficient processing and not above 0.65 to avoid weakening of transverse properties of the part due increasing fibre-fibre contact.

For the pressure, the lower boundary was the minimum pressure a clamping unit of an injection moulding machine can maintain during the compression step, which would be 10 bar in our case. To avoid leakage from the vertical shut-off and to prevent excessive compaction, the maximum pressure and temperature investigated here was limited to 50 bar and 300 °C respectively.

The lowest temperatures used was 280°C as no complete impregnation was possible at 260°C even after 15 min. The impregnation time was limited to 5 min since the preliminary experiments

showed no significant improvement of the impregnation quality and for an industrial process the impregnation time should be as short as possible.

2.4.1 Influence of target fibre volume fraction on fibre distribution

In the photographs of the polished samples, we evaluated different fibre volume fractions, shown in Fig. 4b ii. The global fibre volume fraction, Vf_{global}, represents the averaged Vf over the plate thickness. In the fabric fibre volume fraction, Vf_{fabric}, only the region of the plate where there is fabric was considered as part of the composite. Vf_{tow} is the local Vf of a single tow.

To identify Vf_{target} that yields the most homogeneous fibre distribution, six plates were produced from the Leno fabric with the following impregnation parameters: 5 min impregnation time, temperature T of 300 °C, and a pressure P of 20 or 50 bar to investigate Vf_{target} values of 0.5, 0.6 and 0.65. To observe homogeneity of the fabric distribution in the plate, the difference Vf_{fabric} - Vf_{global} was evaluated. This value would ideally be minimal for a homogeneous distribution of the fabric through the plate thickness.

2.4.2 Influence of fabric architecture on impregnation

To get an indication of the flow front development and flow type, three plates were produced from both fabrics (Leno and Two warp). All plates were produced at the Vftarget leading to the most homogeneous plate discussed in 3.2.1, with a value of 0.65, using a pressure of 50 bar. At 280 °C, one plate was produced using a 1 min impregnation time to observe the impregnation mid-process. Another plate using 5 min impregnation time was produced to achieve a fully impregnated plate. To further improve the final impregnation, a plate was manufactured at 300 °C using 5 min impregnation time. The impregnated and non-impregnated regions of the samples were identified from the photographs with UV light of the polished samples.

2.4.3 Influence of pressure and temperature on tow fibre volume fraction and porosity

To find suitable processing parameters for a plate with uniform Vf_{tow}, and a low and homogeneous porosity, the following processing parameters were compared: For all four plates, the Leno weave fabric was used with Vf_{target} of 0.65, and an impregnation time of 5 min. The plates were made at

280 °C and 300 °C with impregnation pressures of 20 or 50 bar. Vf_{tow} was evaluated from the cross-section area of the tows, A_{tow} [mm²], the linear weight, kTex [kg/km], and the density of the fibres, ρ [g/cm³], as follows, Eq. (9):

$$Vf_{tow} = \frac{kTex/\rho}{A_{tow}} \qquad (9)$$

The tow porosity was calculated with Eq. (10):

$$Porosity_{tow} = \frac{A_{fluo}}{A_{tow}} \qquad (10)$$

where A_{fluo} is the bright fluorescent non-impregnated area from the photographs under UV light and A_{tow} is the area of the tow.

3 Results and discussion

3.1 Dry fabric compaction and saturated through thickness permeability

Fig. 5a shows the compaction curves of the two studied UD glass fabrics. The compaction curves are fitted by a hyperbolic tangent fit [40], Eq. (11).

$$Vf(P) = Vf_0 + (Vf_{max} - Vf_0) \cdot tanh^n\left(\frac{P}{P_{max}}\right) \qquad (11)$$

where P is the pressure, Vf_0 is the minimum fibre volume content, Vf_{max} is the maximum fibre volume content; P_{max} is the maximum pressure and n is a fitting parameter.

The mean Vf of three measurements at pressures of 1, 2, 5, 10, 20 and 50 bar were used for a least-squares fit. In Fig. 5b, the permeability K is shown as a function of the compaction pressure P. The value of K(Vf) was described by a power law [41], and can be combined with Eq. (11) to give K(P) in Eq. (12). The mean permeability of three measurements at four different Vf was used for a least-squares fit.

$$K(P) = A \cdot \left[Vf_0 + (Vf_{max} - Vf_0) \cdot tanh^n\left(\frac{P}{P_{max}}\right)\right]^B \qquad (12)$$

where both A and B are fitting parameters.

All fitting parameters of Eq. (11) and Eq. (12) for the two fabrics are summarised in Table 2.

The coefficient of variation, c_v, of most of the permeability values is below 22 %, except for Two warp fabric at very high fibre volume contents (Vf 0.74 and Vf 0.76) with a c_v above 40 %. In contrast [42], the second benchmark for the experimental determination of the in-plane permeability, c_v within one laboratory was found to be around 15% and 20 % between the partners, which is in good agreement of the c_v reached here for most experiments, considering that we used out of plane measurements at very high Vf. There are several possible reasons for the high c_v values mentioned above as discussed in [43]. First, the fabric layers can shift relative to each other, and this nesting can block the flow in the pinholes between the tows [44, 45]. Second, there could be variations in the fabric areal weight, and third there could be race tracking caused by loss of fibres at the edge of the sample. Since the sample diameter is bigger than the area of the flow in our case, race tracking could be avoided. In the Leno fabric the layers tend to nest in a regular way due to the bigger and rounder tows, leading to a similar arrangement of the pinholes in different samples. In the Two warp fabric the nesting of the layers is much more random due to the smaller and rather flat tows. The Two warp fabric is also more delicate to handle, distortions in the fabric are more likely to occur than in the Leno fabric. These two effects lead to a higher variability of pinhole distribution, leading to a higher variability in the permeability.

Fig. 5 shows that, over the whole pressure range, the compaction in the Two warp fabric is much higher than that of the Leno fabric. This results in lower permeability for the Two warp fabric compared to the Leno fabric. At a typical processing pressure of 20 bar, the Vf of the Two warp is 3% higher with a corresponding permeability that is only 30% of that of the Leno fabric. This difference can be explained by looking at the fabric architecture in Fig. 2. The size of the Leno fabric tows is about four times bigger than that of the Two warp fabric tows, leading to rather round and well separated tows and structured surface of the layer in the Leno fabric. The Leno fabric tows have a high resistance to deformation. This leads to lower compaction and higher permeability in the Leno fabric compared to the Two warp fabric.

With the above measured Vf and permeability values and the viscosity values given in Fig. 2, the impregnation time can be estimated from Eq. (6). Assuming an impregnation length of 5 mm, and

temperature of 280 or 300 °C (resulting in 40 or 15 Pas), and Δp of 10 or 20 bar, the impregnation time for FTA Leno was between 0.35 and 1.6 min, and for the Tissa Two warp between 1.1 and 5.5 min. These values show that an impregnation time of 5 min should result in complete impregnation.

3.2 Impregnation experiments

3.2.1 Influence of target fibre volume fraction on fibre distribution

The Vf_{target} has a big influence on the final distribution of the fabric in the plate. In Fig. 6, the difference between the Vf_{global} and Vf_{fabric} is shown as a function of Vf_{target}. Too low Vf_{target} results in a big difference Vf_{global} - Vf_{fabric}, which shows in a thick polymer layer at the top of the plate. Only with a high Vf_{target} of 0.65 and 300 °C impregnation temperature, this effect is avoided.

This effect is explained by the pressure gradient occurring during the CRTM process described in the introduction. Regardless of the chosen Vf_{target}, the fabric is always compacted with the impregnation pressure in the beginning of the impregnation. From this maximum compressed Vf_{fabric}, the stack is relaxing during the impregnation when the pressure acting on the fabric is decreasing. In Fig. 6 the effect of impregnation pressure is visible as well. For all Vf_{target} the resulting polymer layer is thinner after impregnation at 50 bar compared to 20 bar. This can be explained by the fact that the impregnation time is shorter at 50 bar compared to 20 bar for this fabric, as described in [46], so that there is more time for relaxation of the stack. Overall, it is advantageous for TP CRTM to work at a high Vf_{target} of 0.65 and a high pressure of 50 bar.

3.2.2 Influence of fabric architecture on impregnation

In Fig. 7, images of impregnated plates at Vf_{target} of 0.65 and pressure of 50 bar taken of the two fabrics with and without UV light are shown in order to observe the tow porosity and tow area respectively. Fig. 7a and b show the impregnation status at 280 °C after 1 min. In Fig. 7a, the PA6 (in black) already penetrated the Leno fabric throughout the plate thickness, but without penetrating the centre of the tows, indicating dual scale flow. In Fig. 7b, the PA6 impregnated four layers of the Two warp fabric completely, just starting with the fifth layer, whose boundary is indicated by the blue dotted line. Here the dual scale flow appears to be much less pronounced, leading to

a layer by layer impregnation. Fig. 7c and d show the impregnation state at 280 °C after 5 min. In Fig. 7c, the tow porosity is decreasing to 0.1%, a reasonable value for a structural part with an impregnation time of 5 min. For the Two warp fabric in Fig. 7d, the flow front progressed one layer further, now being at 5 fully impregnated layers, the sixth layer just at the beginning of the impregnation and the dry seventh layer indicated by the blue dotted line. To see if the impregnation quality improves, the experiment was repeated at 300 °C and 5 min impregnation time. Due to the resulting lower melt viscosity, in Fig. 7e, the porosity in the Leno fabric could be further decreased to 0.05%, and is evenly distributed in the plate, whereas all the seven layers of the Two warp fabric in Fig. 7f are impregnated, showing a porosity of 1.1% all concentrated in the seventh layer.

The dual scale impregnation in the Leno fabric shown in Fig. 7a originates from its lower compliance compared to the Two warp fabric. In addition, the regular arrangement of tows in adjacent layers leaving connected flow channels between the tows is in favour of the dual scale flow. In the Two warp fabric the layers can move against each other, thus closing flow paths and leading to a more uniform material that is impregnated layer by layer.

These results elucidate the principal differences of the impregnation mechanism. In terms of impregnation time, the Leno fabric is favourable. Considering the mechanical properties, it is advantageous to have the porosity evenly distributed in the part and not concentrated on a single edge.

3.2.3 Influence of pressure and temperature on bundle fibre volume fraction and porosity in Leno woven fabric

Finally, the influence of processing pressure and temperature on the porosity and the gradient of Vf_{tow} through the thickness of the plate was investigated. All plates were manufactured at the Vf_{target} leading to the most homogeneous plate as explained in 3.2.1, of 0.65 and with the impregnation time of 5 min. For all the investigated pressures and temperatures, there is a general trend of increasing Vf_{tow} from the first layer to be impregnated to the last, shown in Fig. 8a. This is because according to Terzaghi's law [27], the pressure on the fabric layers starts to decrease as soon as they are fully impregnated and start to relax. This effect, albeit small, is quantifiable in the experiments. The first layer has the most time to relax and thus the lowest Vf_{tow}. This gradient

should be as low as possible, and this is the case for the impregnation at 280°C and 20 bar. The average tow porosity per layer is shown in Fig. 8b. For all the investigated cases, it is below 1%, with a trend of being highest in the first and fourth layer. It is noted, that with the Leno fabric the porosity is always located in the intra tow and never inter tow region. From the investigated processing parameters, 300°C and 50 bar resulted in minimal porosity.

3.3 Processing window

The various impregnation experiments have led to the following conclusions: The TP CRTM process only makes sense for parts with a high Vf_{target}, since the high processing pressures lead to a high compaction of the fabric, which only marginally relaxes. The fabric architecture is crucial in resisting the high compaction forces while maintaining an inter tow spacing which promotes dual scale flow. Dual scale flow is advantageous for this process in terms of impregnation time and porosity distribution. In contrast to the CRTM process with curing resins where the air in the middle of the bundles cannot escape, in the thermoplastic matrix some air can be dissolved at high pressure and temperature [47]. The dissolution of air possibly further reduces the viscosity [48], enhancing the impregnation. The best impregnation parameters for the Leno weave fabric to achieve a minimal Vf_{tow} gradient through the thickness are a Vf_{target} of 0.65, 280 °C, 20 bar and an impregnation time of 5 min. The lowest porosity was reached with Vf_{target} of 0.65, 300 °C, 50 bar and an impregnation time of 5 min. However, in the industrial application process it would be easier to implement 280°C and 20 bar, since the viscosity of the PA6 increases from 15 to 40 Pas, which is an advantage regarding the sealing technique of the mould.

4 Conclusions

We investigated the impregnation mechanisms in a TP CRTM process of glass fabrics with low viscosity thermoplastics, and give an indication about its feasibility. With the characterisation of the compaction and permeability of two glass fabrics under the high pressures needed for the direct thermoplastic impregnation, the Leno fabric appeared to be a favourable architecture for TP CTRM. From the impregnation experiments, we came to not obvious conclusions: first, we need a high Vf_{target} for this process to avoid a polymer layer on one side of the plate; second, the fabric architecture can lead to more or less pronounced dual scale flow. Third, pronounced dual

scale flow is advantageous for the process, as it is much faster, and a low tow porosity can be achieved. We found a processing window for the Leno fabric with the low viscosity polyamide at Vf_{target} 0.65, 280-300 °C, 20-50 bar and 5 min impregnation time, with the lowest porosity at 300°C and 50 bar. In the end, the parameters are a trade-off between the impregnation quality with the porosity and Vf_{tow} gradient as indicators, and the process robustness, mainly related with the sealing of moving parts at high temperatures and low melt viscosity.

Overall, we found the process to be attractive for industrial production of thermoplastic composites and gave a first indication of the processing window. The fabric architecture plays a key role and needs to be adapted to the process to withstand a high processing pressure while maintaining open flow channels. With this work, relevant conclusions for the specification of dedicated textile architectures and the specification of variothermal tooling and associated equipment could be drawn to open the way towards industrial validation. A preliminary cost and life cycle analysis for industrial scale up [49] showed that the share of the process energy is 12 % regarding cost and below 25 % regarding environmental impact indicators in the categories of resources, ecosystem quality and human health, evaluated according to [50].

With impregnation times of 5 min and novel heating systems like induction [51], cycle times around 15 min for a fabric reinforced net shaped part including functionalities may become a realistic proposition for the automated production of fibre reinforced thermoplastic composites.

5 Acknowledgements

We would like to acknowledge C. Schneeberger from Tissa Glasweberei AG, Switzerland, and T. Bischoff from FTA Albstadt GmbH, Germany, for providing the textiles and G. Orange from Solvay for providing the PA6. This research was supported by the Swiss Competence Center for Energy Research (SCCER) Efficient Technologies and Systems for Mobility, funded by the Swiss Innovation Agency, Innosuisse.

6 References

1. Pearce, N.R.L., J. Summerscales, and F.J. Guild, *Improving the resin transfer moulding process for fabric-reinforced composites by modification of the fabric architecture.* Composites Part A: Applied Science and Manufacturing, 2000. **31**(12): p. 1433-1441.
2. Kracke, C., et al., *Interaction of textile variability and flow channel distribution systems on flow front progression in the RTM process.* Composites Part A: Applied Science and Manufacturing, 2018. **106**: p. 70-81.
3. Poodts, E., et al., *Fabrication, process simulation and testing of a thick CFRP component using the RTM process.* Composites Part B: Engineering, 2014. **56**: p. 673-680.
4. Han, S.H., et al., *Study on high-speed RTM to reduce the impregnation time of carbon/epoxy composites.* Composite Structures, 2015. **119**: p. 50-58.
5. Merotte, J., P. Simacek, and S.G. Advani, *Resin flow analysis with fiber preform deformation in through thickness direction during Compression Resin Transfer Molding.* Composites Part A: Applied Science and Manufacturing, 2010. **41**(7): p. 881-887.
6. Verleye, B., et al., *Simulation and experimental validation of force controlled compression resin transfer molding.* Journal of Composite Materials, 2011. **45**(7): p. 815-829.
7. Bhat, P., et al., *Process analysis of compression resin transfer molding.* Composites Part A: Applied Science and Manufacturing, 2009. **40**(4): p. 431-441.
8. Masania, K.B., B.; Dransfeld, C. *The compression resin transfer moulding process for efficient composite manufacture*. in *The 19th International Conference on Composite Materials*. 2013. Montreal, Canada.
9. Deinzer, G., et al., *Audi Ultra-RTM: A technology for high performance and cost effective CFRP part for high volume production*, in *ECCM17 - 17th European Conference on Composite Materials*. 2016: Munich, Germany.
10. Michaud, V., *A Review of Non-saturated Resin Flow in Liquid Composite Moulding processes.* Transport in Porous Media, 2016. **115**(3): p. 581-601.
11. Geissberger, R., et al., *Rheological modelling of thermoset composite processing.* Composites Part B: Engineering, 2017. **124**: p. 182-189.
12. Roux, M., et al., *Thermoplastic carbon fibre-reinforced polymer recycling with electrodynamical fragmentation: From cradle to cradle.* Journal of Thermoplastic Composite Materials, 2015. **30**(3): p. 381-403.
13. Shi, H., I.F. Villegas, and H.E.N. Bersee, *Strength and failure modes in resistance welded thermoplastic composite joints: Effect of fibre–matrix adhesion and fibre orientation.* Composites Part A: Applied Science and Manufacturing, 2013. **55**: p. 1-10.
14. Schaefer, P.M., et al., *Analysis and improved process response prediction of laser- assisted automated tape placement with PA-6/carbon tapes using Design of Experiments and numerical simulations.* Composites Part A: Applied Science and Manufacturing, 2017. **96**: p. 137-146.
15. Qureshi, Z., et al., *In situ consolidation of thermoplastic prepreg tape using automated tape placement technology: Potential and possibilities.* Composites Part B: Engineering, 2014. **66**: p. 255-267.
16. Boehm, R., et al., *Thermoplastic Composites Reinforced with Textile Grids: Development of a Manufacturing Chain and Experimental Characterisation.* Applied Composite Materials, 2013. **20**(6): p. 1077-1096.

17. Guillon, D., A. Lemasçon, and C. Callens, *QSP®: An innovative process based on tailored preforms for low cost and fast production of optimized thermoplastic composite parts*, in *ECCM17 - 17th European Conference on Composite Materials*. 2016: Munich, Germany.
18. Wedhorn, L. and R. Ebeling, *Quilted Stratum Process for High-performance CFRP Production.* Lightweight Design worldwide, 2017. **2017**(1).
19. Zingraff, L., et al., *Resin transfer moulding of anionically polymerised polyamide 12.* Composites Part a-Applied Science and Manufacturing, 2005. **36**(12): p. 1675-1686.
20. Maazouz, A., K. Lamnawar, and M. Dkier, *Chemorheological study and in-situ monitoring of PA6 anionic-ring polymerization for RTM processing control.* Composites Part A: Applied Science and Manufacturing, 2018. **107**: p. 235-247.
21. Solvay, *High Fluidity PA6 (HF XS1480) for Consolidated Laminate*. 2014.
22. Babeau, A., et al., *Modeling of heat transfer and unsaturated flow in woven fiber reinforcements during direct injection-pultrusion process of thermoplastic composites.* Composites Part A: Applied Science and Manufacturing, 2015. **77**: p. 310-318.
23. Cazaux, G., *Feasability of LCM processes in the elaboration of continuous fiber-reinforced composite with a thermoplastic polyamid matrix*. 2016, Université du Havre.
24. Salvatori, D., *Strategies for faster impregnation in melt thermoplastic resin transfer molding process*, in *Material Science and Engineering*. 2018, EPFL: Lausanne.
25. Orange, G., et al., *Development of composite parts with RTM process based on new high fluidity thermoplactic polymers*. 2014.
26. Darcy, H., *Les Fontaines Publiques de la Ville de Dijon: Exposition et Application des Principes a Suivre et des Formulesa Employer dans les Questions de Distribution d'Eau*. 1856. 647.
27. Terzaghi, K. and R.B. Peck, *Soil mechanics in engineering practice*. 1967, New York: Wiley.
28. Klunker, F., M. Danzi, and P. Ermanni, *Fiber deformation as a result of fluid injection: modeling and validation in the case of saturated permeability measurements in through thickness direction.* Journal of Composite Materials, 2015. **49**(9): p. 1091-1105.
29. Simacek, P., J. Merotte, and S.G. Advani, *Compression Resin Transfer Molding Simulation for Net Shape Manufacturing of Composite Structures for Automotive Applications.* Sampe Journal, 2016. **52**(1): p. 11.
30. Pham, X.-T., F. Trochu, and R. Gauvin, *Simulation of Compression Resin Transfer Molding with Displacement Control.* Journal of Reinforced Plastics and Composites, 1998. **17**(17): p. 1525-1556.
31. Keller, A., C. Dransfeld, and K. Masania, *Flow and heat transfer during compression resin transfer moulding of highly reactive epoxies.* Composites Part B: Engineering, 2018. **153**: p. 167-175.
32. Salvatori, D., et al., *Permeability and capillary effects in a channel-wise non-crimp fabric.* Composites Part A: Applied Science and Manufacturing, 2018. **108**: p. 41-52.
33. LeBel, F., et al., *Prediction of optimal flow front velocity to minimize void formation in dual scale fibrous reinforcements.* International Journal of Material Forming, 2014. **7**(1): p. 93-116.
34. Ruiz, E., et al., *Optimization of injection flow rate to minimize micro/macro-voids formation in resin transfer molded composites.* Composites Science and Technology, 2006. **66**(3): p. 475-486.

35. Orange, G.C.-C., S., Maupetit, J. *Thermoplastic melt impregnation of composite laminates by injection-compression process*. in *The 14th international conference on flow processing in composite materials*. 2018. Lulea, Sweden.
36. Dijkstra, D.J., *Guidelines for Rheological Characterization of Polyamide Melts (IUPAC Technical Report)*, in *Chemistry International -- Newsmagazine for IUPAC*. 2009. p. 24.
37. Merhi, D., et al., *Transverse permeability of chopped fibre bundle beds.* Composites Part a-Applied Science and Manufacturing, 2007. **38**(3): p. 739-746.
38. Michaud, V. and A. Mortensen, *Infiltration processing of fibre reinforced composites: governing phenomena.* Composites Part a-Applied Science and Manufacturing, 2001. **32**(8): p. 981-996.
39. Hayes, B.S. and L.M. Gammon, *Optical microscopy of fiber reinforced composites.* 2010.
40. Merotte, J., P. Simacek, and S.G. Advani, *Flow analysis during compression of partially impregnated fiber preform under controlled force.* Composites Science and Technology, 2010. **70**(5): p. 725-733.
41. Ouahbi, T., et al., *Modelling of hydro-mechanical coupling in infusion processes.* Composites Part A: Applied Science and Manufacturing, 2007. **38**(7): p. 1646-1654.
42. Arbter, R., et al., *Experimental determination of the permeability of textiles: A benchmark exercise.* Composites Part A: Applied Science and Manufacturing, 2011. **42**(9): p. 1157-1168.
43. Endruweit, A. and A.C. Long, *9 - Understanding variability in the permeability of non-crimp fabric composite reinforcements*, in *Non-Crimp Fabric Composites*, S.V. Lomov, Editor. 2011, Woodhead Publishing. p. 216-241.
44. Yun, M., et al., *Stochastic modeling of through the thickness permeability variation in a fabric and its effect on void formation during Vacuum Assisted Resin Transfer Molding.* Composites Science and Technology, 2017. **149**(Supplement C): p. 100-107.
45. Yang, B., S. Wang, and Y. Wang, *Effect of Nesting in Laminates on the Through-Thickness Permeability of Woven Fabrics.* Applied Composite Materials, 2018. **25**(5): p. 1237-1253.
46. Studer, J., et al. *Thermoplastic composites manufacturing: Direct melt impregnation of fabrics through injection moulding*. in *15th European-Japanese Symposium on Composite Materials : New Generations of Composite*. 2017. London, UK.
47. Sato, Y., et al., *Solubilities and diffusion coefficients of carbon dioxide and nitrogen in polypropylene, high-density polyethylene, and polystyrene under high pressures and temperatures.* Fluid Phase Equilibria, 1999. **162**(1-2): p. 261-276.
48. Gendron, R. and L.E. Daigneault, *Continuous extrusion of microcellular polycarbonate.* Polymer Engineering & Science, 2003. **43**(7): p. 1361-1377.
49. Berret, L., *Life cycle assessment and cost analysis of novel manufacturing processes for thermoplastic composites*, in *Material Science and Engineering*. 2018, EPFL.
50. De Schryver, A.M., et al., *Characterization Factors for Global Warming in Life Cycle Assessment Based on Damages to Humans and Ecosystems.* Environmental Science & Technology, 2009. **43**(6): p. 1689-1695.
51. Bayerl, T., et al., *The heating of polymer composites by electromagnetic induction – A review.* Composites Part A: Applied Science and Manufacturing, 2014. **57**: p. 27-40.

1

List of Tables

Table 1: Overview of the impregnation experiments and the different evaluation methods that were used.

Experiment used to study			Impregnation parameter				
Influence of Vf_{target} 3.2.1	Influence of Fabric 3.2.2	Influence of P, T 3.2.3	Fabric	Vf_{target}	Temp [°C]	P [bar]	Time [min]
x			Leno	0.5	300	20	5
x			Leno	0.6	300	20	5
x		x	Leno	0.65	300	20	5
x			Leno	0.5	300	50	5
x			Leno	0.6	300	50	5
x	x	x	Leno	0.65	300	50	5
	x		Leno	0.65	280	50	1
	x		Leno	0.65	280	50	5
	x		Two warp	0.65	300	50	5
	x		Two warp	0.65	280	50	1
	x	x	Two warp	0.65	280	50	5
		x	Leno	0.65	280	20	5

Table 2: Fitting parameters of the fibre volume fraction Vf (Eq. (11)) and through thickness permeability (Eq. (12)) as function of compaction pressure.

Fabric weave	Vf_0	Vf_{max}	*n*	P_{max} *[bar]*	*A*	*B*
Leno	0.2	0.795	0.08	63	1.5E-13	-6.78
Two warp	0.15	0.83	0.078	63	8.13E-14	-5.26

List of Figures

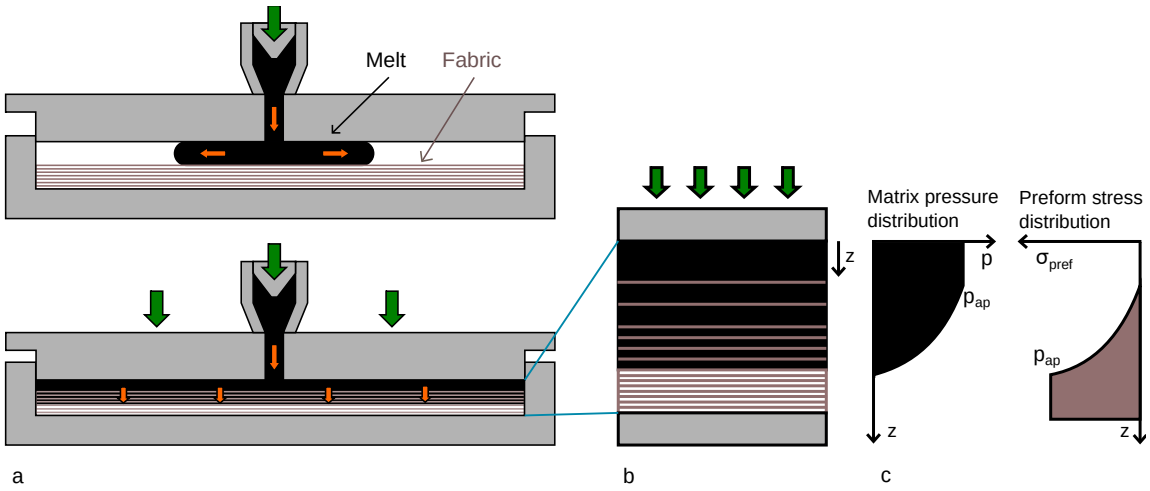

Fig. 1. Concept for TP CRTM tool using a vario-thermal injection-compression moulding process a) Injection: Melt is injected in a gap above the fabric; b) Impregnation: a constant pressure is applied over the fabric surface during the compression step, leading to a gradient in the fibre volume content through the thickness during impregnation. c) Schematically shows the pressure distribution between the fabric and matrix during impregnation.

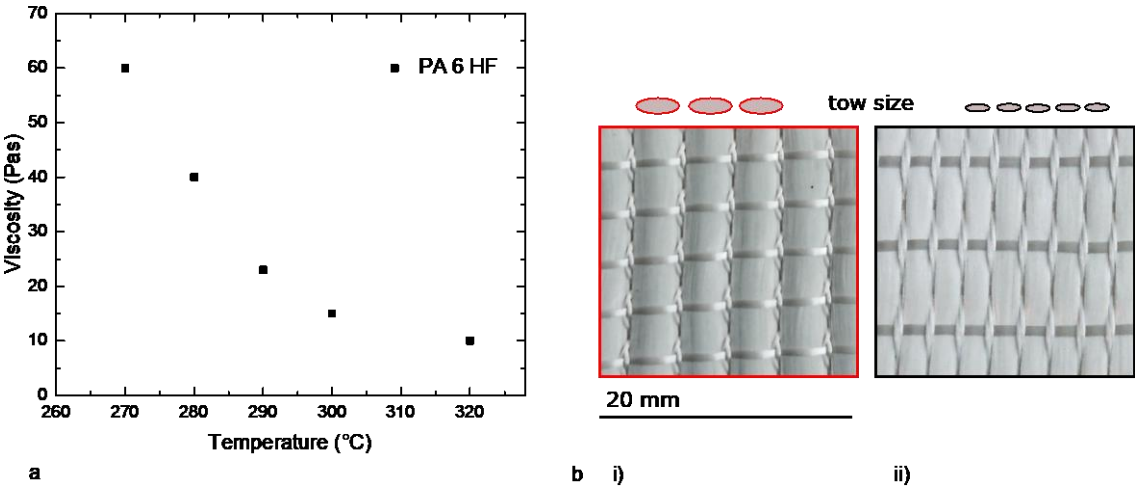

Fig. 2. a) Viscosity of the low viscosity PA6, measured with a cone-plate rheometer at a shear rate of $10s^{-1}$ [35]. b) Structure of the unidirectional glass fabrics and their corresponding tow sizes: i) Leno weave, 1280 g/m², 4800 tex; ii) Two warp weave, 600 g/m², 1200 tex.

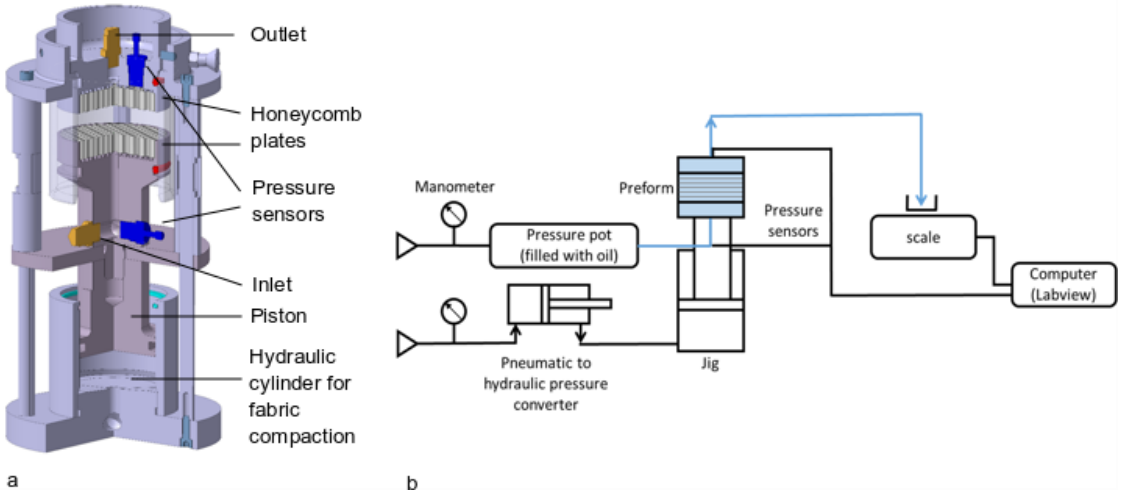

Fig. 3. a) Schematic of the through-thickness permeability jig and b) the experimental setup.

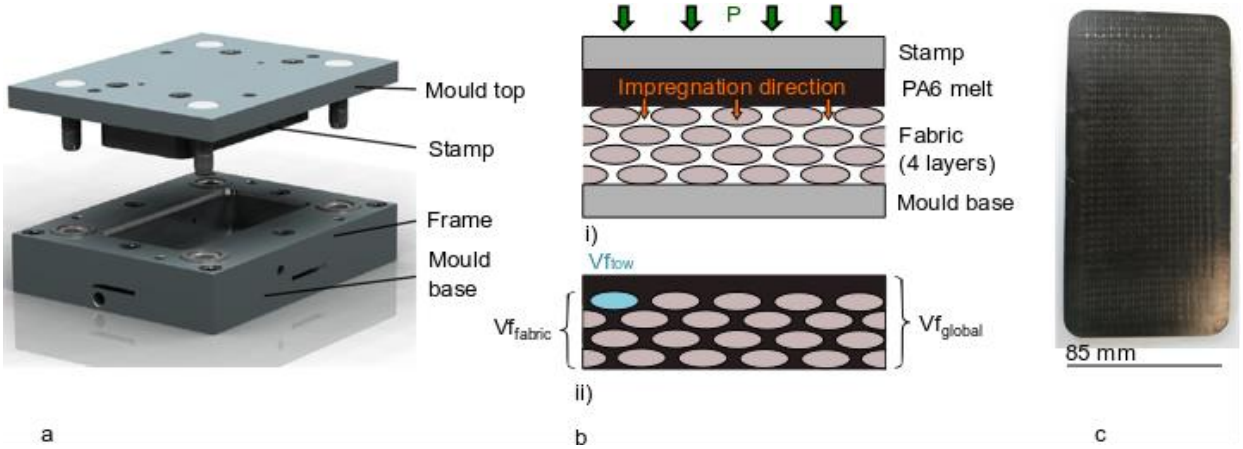

Fig. 4. a) Mould used in the impregnation experiment; bi) Schematic of the experiment, with impregnation direction from top to bottom; bii) Definition of the different fibre volume contents; Vf_{global} is the global Vf in the whole plate, Vf_{fabric} is the Vf in the part of the plate where there is fabric, Vf_{tow} is the Vf inside a tow; c) Impregnated plate after demoulding.

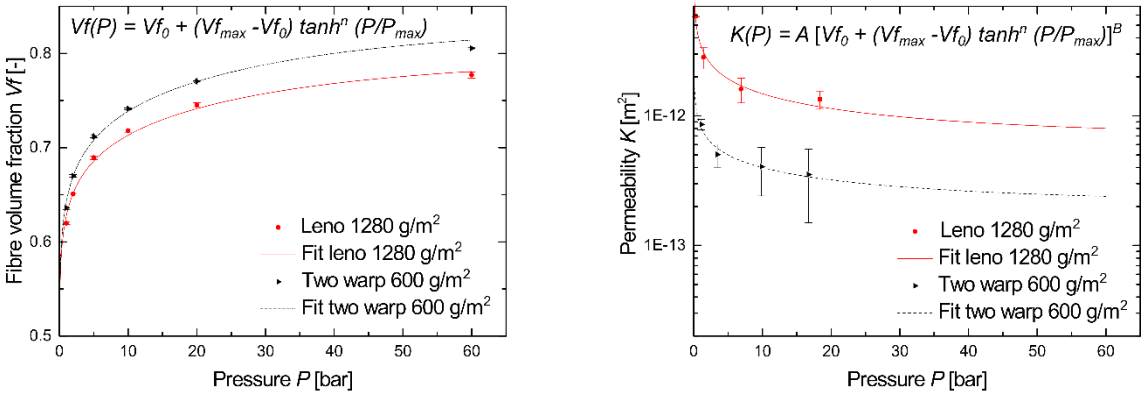

a b

Fig. 5. Fabric characterisation: a) Dry fabric compaction with hyperbolic tangent fit and b) saturated permeability with power law fit; showing the higher compaction and the corresponding lower permeability of the Two warp fabric.

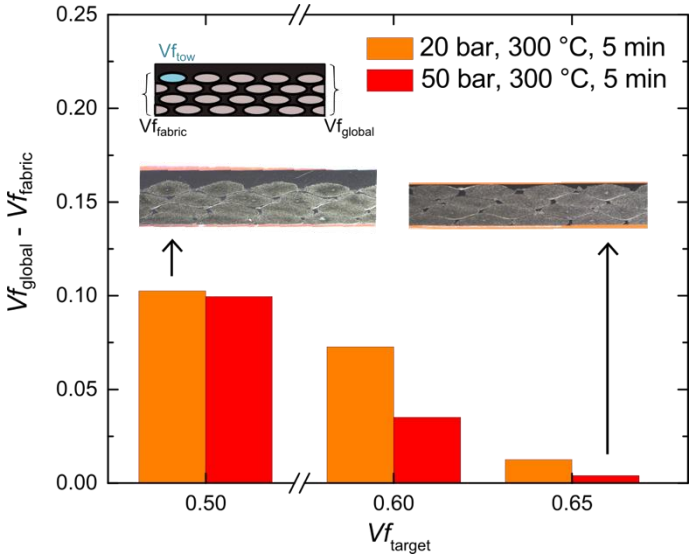

Fig. 6. Influence of Vf_{target} on the Vf distribution in the plate for the Leno weave, showing that a Vf_{target} lower than 0.65 leads to a polymer layer and a higher Vf_{fabric}.

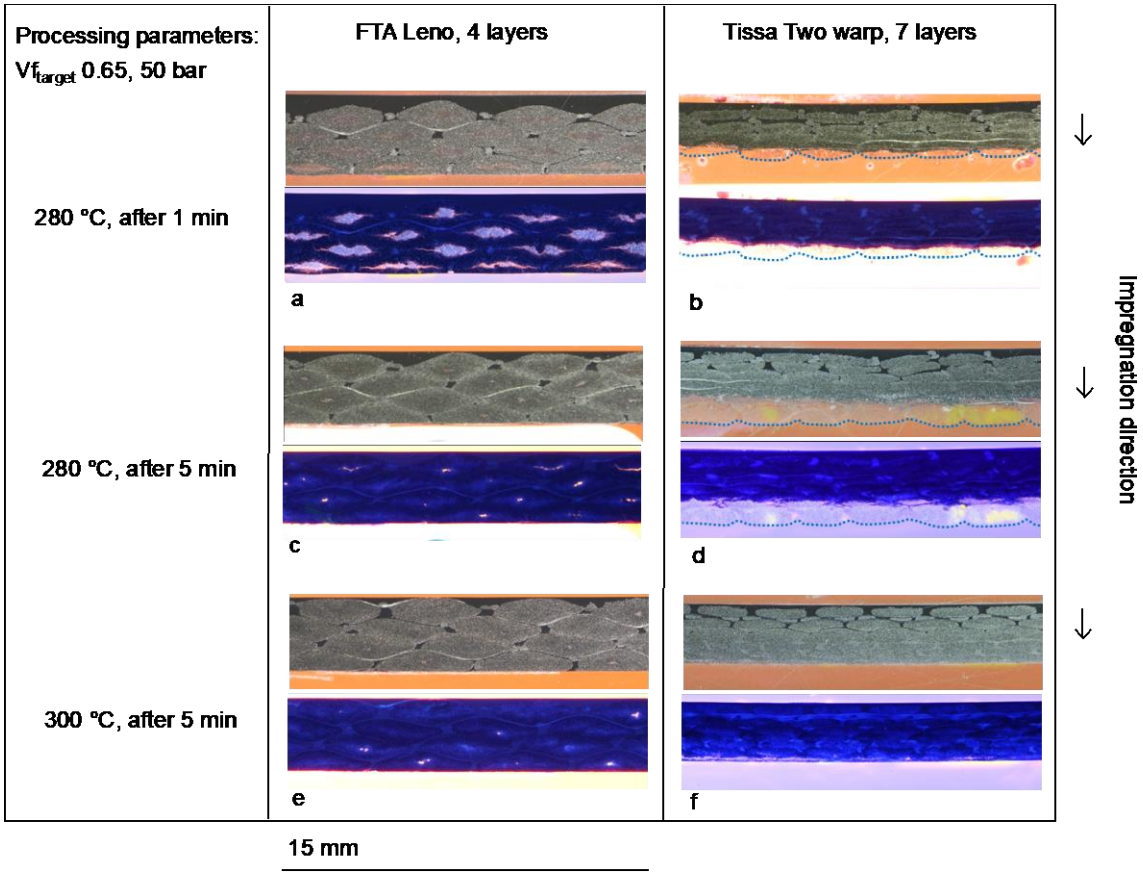

Fig. 7. Micrographs without (above) and with (below) UV light from impregnation trials. They show dual scale impregnation in the Leno fabric a) vs. single scale impregnation in the Two warp fabric b), where the dotted blue lines indicate impregnated layers) when the impregnation is interrupted after 1 min at 280°C. After 5 min at 280 °C the Leno fabric is almost completely impregnated with little porosity distributed in the middle of the tows c), while in the Two warp fabric a clear flow front is visible d). When impregnating at 300 °C, both fabrics can be completely impregnated. In the Leno fabric, the porosity is distributed in the plate e), where in the Two warp the porosity is concentrated on one edge.

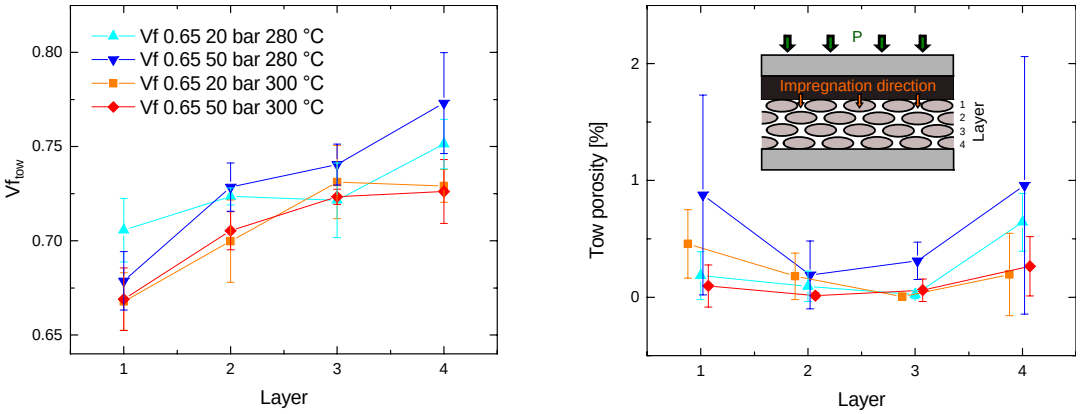

Fig. 8. a) Gradient of Vf_{tow} and b) porosity through the thickness, with the processing parameters at Vf_{target} 0.65, 50 bar and 300 °C resulting in the lowest porosity and gradient in Vf_{tow}.